Theoretical and Applied Climatology (2024) 155:3281–3296
https://doi.org/10.1007/s00704-023-04809-2

RESEARCH

A spatiotemporal oscillator model for ENSO

Yaokun Li[1]

Received: 13 August 2023 / Accepted: 17 December 2023 / Published online: 3 January 2024

Abstract
A spatiotemporal oscillator model for El Niño/Southern Oscillation (ENSO) is constructed based on the thermodynamics and thermocline dynamics. The model is enclosed by introducing a proportional relationship between the gradient in sea surface temperature (SST) and the oceanic zonal current and can be transformed into a standard wave equation that can be decomposed into a series of eigenmodes by cosine series expansion. Each eigenmode shows a spatial mode that oscillates with its natural frequency. The first spatial mode, that highlights SST anomaly (SSTA) contrast between the eastern and western Pacific—a fundamental characteristic of the eastern Pacific (EP) El Niño events, oscillates with a natural period of around 4.6 years, consistent with the quasi-quadrennial (QQ) mode. The second spatial mode, that emphasizes SSTA contrast between the central and the eastern, western Pacific—a basic spatial structure of the central Pacific (CP) El Niño events, oscillates with a natural period of 2.3 years that is half of the first natural period. It is also consistent with the quasi-biennial (QB) modes. The combinations of the eigenmodes with different weights can feature complex spatiotemporal variations in SSTAs. In open ocean that is far away from the coastlines, the model can predict waves propagating both eastward and westward. Besides, the net surface heating further complicates the temporal variations by exerting forced frequencies. The model unifies the temporal and spatial variations and may provide a comprehensive viewpoint for understanding the complex spatiotemporal variations of ENSO.

1 Introduction

The El Niño/Southern Oscillation (ENSO) phenomenon, manifested by the great swings of large-scale sea surface temperature anomalies (SSTAs) over the equatorial central to eastern Pacific oceans, is a major source of interannual global shifts in climate patterns and weather activities (Jin 2022). ENSO originates in the tropical Pacific through interactions between the ocean and the atmosphere, but its environmental and socioeconomic impacts are felt worldwide (McPhaden et al. 2006). Based on the continuous observation in the tropical Pacific by the Tropical Ocean Global Atmosphere (TOGA) program, our understanding of ENSO has made significant process (Wang and Picaut 2004; McPhaden et al. 2010) and has continued to evolve as new layers of complexity that refers to the diversity in spatial patterns, amplitude, and temporal evolution (Timmermann et al. 2018).

To deal with the temporal evolution, it is natural to highlight the variation of SSTAs in the central to eastern Pacific. This naturally leads to the neglect of the west-east gradients in SSTAs, hence the spatial structure. The delayed oscillator model (Suarez and Schopf 1988; Battisti and Hirst 1989) introduces a time delay term to include the effects of the oceanic Rossby and Kelvin wave transit that had been noticed by McCreary (1983) in a simple coupled ocean-atmosphere model. The recharge oscillator (RO) model (Jin 1997) combines SST dynamics and oceanic adjustment dynamics into a coupled basin-wide RO framework that relies on the non-equilibrium between the zonal mean equatorial thermocline depth and the wind stress. There are other types of theoretical models to highlight different physical processes, such as the western Pacific oscillator model (Weisberg and Wang 1997), the advective-reflective oscillator model (Picaut et al. 1997), and the unified oscillator model (Wang 2001). The recent review by Wang (2018) explicitly compared the similarities and differences among these oscillator models. Specific to the RO framework, incorporating seasonality, nonlinearity, and multiscale processes, it allows for basic understanding

✉ Yaokun Li
liyaokun@bnu.edu.cn

[1] College of Global Change and Earth System Science, Faculty of Geographical Science, Beijing Normal University, Beijing 100875, China

of how key physical processes determine ENSO's properties, such as its amplitude, periodicity, phase-locking, asymmetry, and nonlinear rectification onto the mean state (Jin et al. 2020). For example, modified parameter RO models had reproduced the main phase-locking characteristics found in observation and suggested that seasonal modulation of the coupled stability is responsible for ENSO phase locking to the annual cycle (An and Jin 2011; Stein et al. 2014; Chen and Jin 2020). The state-dependent stochastic forcing in RO model enhances the instability of ENSO and its ensemble spread generates asymmetry in the predictability (Jin et al. 2007; Levine and Jin 2010). RO framework with nonlinear advection may explain ENSO amplitude modulations and irregularity by applying the concept of homoclinic and heteroclinic connections (Jin 1998; Timmermann and Jin 2002; Timmermann et al. 2003).

To deal with the spatial diversity, theoretical and statistical analyses that are based on the observation and the model simulating are often used to interpret the observed two types of ENSO, now widely known as the central Pacific (CP) and the eastern Pacific (EP) El Niño events (Larkin and Harrison 2005a, b; Ashok et al. 2007; Kao and Yu 2009; Kug et al. 2009). For example, linear eigen-analysis of the Zebiak-Cane (ZC) model shows that there are two leading ENSO modes that have periods of around 4 and 2 years and thereby referred to the quadrennial (QQ) and quasi-biennial (QB) modes, respectively (Bejarano and Jin 2008; Xie and Jin 2018). This may be further demonstrated by natural random variations in a multivariate, "patterns-based," red noise model (Newman et al. 2011). Besides, new indices, such as the trans-Niño index (TNI) which is given by the difference in normalized SSTAs between NINO 1 + 2 and NINO 4 regions (Trenberth and Stepaniak 2001) and the E and C indices that are based on the first two empirical orthogonal function (EOF) modes of tropical Pacific SSTAs (Takahashi et al. 2011), may also be introduced to describe the diversity of patterns. Recently, Xie et al. (2020) further defined new indices of ENSO diversity that explicitly account for the nonlinear convection-SST sensitivity. The recent review by Capotondi et al. (2020) explicitly summarized the key aspects of ENSO's spatial diversity.

The previous investigations had highlighted either the spatial or the temporal variations and had greatly promoted our understanding ENSO complexity. Recent works have attempted to systematically discuss the complex spatiotemporal pattern diversity (STPD). For example, Fang and Mu (2018) extended the RO model to a three-region conceptual model to describe the entire western, central, and eastern equatorial Pacific. Takahashi et al. (2019) suggested that it is sufficient to produce the two types of ENSO in the nonlinear RO model. Geng et al. (2020) constructed a nonlinear two-box RO model to account for event diversity of ENSO. Chen et al. (2022) developed a three-region multiscale stochastic conceptual model for the ENSO complexity by introducing intra-seasonal and decadal components. The model was further developed to realistically reproduce the strength, occurrence frequency, and spatiotemporal patterns of both EP and CP Niño events (Chen and Fang 2023). Besides, the model is also developed to assess the predictability and quantify the forecast uncertainty of ENSO complexity (Fang and Chen 2023). More recently, Geng and Jin (2023a, b) further investigated the dynamics of ENSO diversity within a ZC-type model and suggested that the diversity is fundamentally generated by deterministic nonlinear pathways to chaos via the period-doubling route and, more prevailingly, the subharmonic resonance route with the presence of a seasonally varying basic state. These works are basically the extension of the classic RO framework by introducing more variables. The spatial patterns are basically represented by two SSTA variables that are predetermined in advance. Therefore, as Jin (2022) proposed the scientific question in a recent review paper—can we achieve a conceptual understanding of ENSO STPD through a systematic investigation of various contributing sources in a similar way to the simple RO model for our understanding of the basic dynamics of ENSO?

To answer this question and to better understand ENSO STPD, this paper tries to provide a systematic view to integrate the spatial and temporal variations by introducing a spatiotemporal oscillator model that stands on the shoulders of the previous successes. This paper is organized as below. Following this introduction section, the spatiotemporal oscillator model is established by applying reasonable assumptions to link the SSTA gradients with the zonal oceanic current anomaly in Section 2. The analytic solution is derived in Section 3. The solution suggests that SSTA STPD can be decomposed into spatial modes associated with natural oscillations. The first two spatial modes and their corresponding natural oscillations, as well as the different combinations of the two modes, are discussed in Section 4. The results show that they can feature the EP and CP El Niño events with complex temporal variations. The model's assumptions and the propagation features are discussed in Section 5. Finally, a conclusion ends the paper in Section 6.

2 The spatiotemporal oscillator model

SSTAs for the central and eastern Pacific must be considered for capturing the essence of the CP and EP patterns (Jin 2022). However, if just introducing two variables to represent the SSTAs in the central and the eastern Pacific (e.g., T_C and T_E), it will only follow the existing RO framework and make it more complicated. Besides, comparing with the traditional practice that introduced two variables to represent the central and eastern Pacific SSTAs that naturally lose the spatial distribution, the treatment that deals

with the continuous SSTAs in the tropical Pacific will be more precise and can naturally analyze the spatial variations. Therefore, to better describe the spatiotemporal variations in SSTAs, let us start with the thermodynamic equation for the upper ocean mixed layer (Deser et al. 2010)

$$\frac{\partial T}{\partial t}+u\frac{\partial T}{\partial x}+v\frac{\partial T}{\partial y}+w\frac{T-T_b}{H}=\frac{1}{\rho C_p H}Q \tag{1}$$

where T is the mixed layer temperature (equal to the SST), u, v are the zonal, meridional currents in the mixed layer, respectively, w is the vertical velocity in the mixed layer, T_b is the temperature of the water at depth that is entrained into the mixed layer, $H = 50$m (Jin et al. 2020) is the mixed layer depth, ρ is the density of the seawater, C_p is the heat capacity, and Q is the net surface heat flux.

Equation (1) contains nonlinear advection terms and is not convenient for theoretical analysis. Based on the budget analysis of the SSTAs from the ocean reanalysis data set, a simplified SSTA equation for ENSO (e.g., Kang et al. 2001) can be derived as

$$\frac{\partial T\prime}{\partial t}+u\prime\frac{\partial \overline{T}}{\partial x}+K_h h\prime=\frac{1}{\rho C_p H}Q\prime\triangleq Q\prime \tag{2}$$

where $T\prime$ is the SSTA, $u\prime$ is the anomalous zonal current, $h\prime$ is the thermocline depth anomaly (TDA), $Q\prime$ is the net surface heat flux anomaly, $\overline{T}$ is the climatological monthly mean SST, and K_h represents the delayed response of the thermocline depth anomalies to the local wind stress forcing or the ocean dynamic feedback from anomalous zonal advection and vertical heat advection associated with the discharge/recharge of equatorial heat content (Jin et al. 2020). Equation (2) retains the main contributing factors to SST variations and similar forms of Eq. (2) have been widely used in theoretical studies of ENSO (Hirst 1986, 1988; Battisti 1988; Battisti and Hirst 1989; Wakata and Sarachik 1991; Neelin and Jin 1993; Jin 1996). Actually, it is also a simplified version of the thermodynamic equation in ZC model (Zebiak and Cane 1987). Here it must be pointed out that the term $K_h h\prime$ is given an opposite sign comparing with previous studies. As Battisti and Hirst (1989) pointed out, changes in $h\prime$ can be written in terms of the local contribution and the remote contribution. The former contributes to the local instability growth, while the latter works a phase transition mechanism which may be either the reflected Kelvin wave at the western ocean boundary (Battisti and Hirst 1989) or the recharge-discharge of the equatorial heat content (Jin 1997). The local instability growth effect can finally be parameterized by SSTA and hence having the same sign with the SSTA variations. The phase transition mechanism and the local response have the opposite sign (Battisti and Hirst 1989). Therefore, the phase transition mechanism and the SST variations have the opposite sign. To highlight the phase transition mechanism, the local instability growth, a component of the Bjerknes positive feedback is neglected in this investigation. It can be considered and analyzed in the future. The value for K_h may vary from $3.5\times10^{-9}\mathrm{Km}^{-1}\mathrm{s}^{-1}$ (Hirst 1986, 1988) to $1.7\times10^{-8}\mathrm{Km}^{-1}\mathrm{s}^{-1}$ (Kang and An 1998) and may also vary with y (e.g., as Kang and An (1998) and Kang et al. (2001) suggested, it has a large value near the equator and a small value off the equator). A moderate value, namely, $K_h = 1.0\times10^{-8}\mathrm{Km}^{-1}\mathrm{s}^{-1}$ is specified in this investigation. Equation (2) may become a simpler and more commonly used form if replacing the net surface heat flux with a Newtonian cooling $-\alpha T\prime$ where $\alpha > 0$ is the damping coefficient.

The thermocline depth is another variable that needs to be considered for understanding ENSO dynamics (Jin 1997). This oceanic dynamical component has been successfully described by a 1.5-layer linear reduced gravity model (Zebiak and Cane 1987). It can be written as

$$\frac{\partial h\prime}{\partial t}+\overline{u}\frac{\partial h\prime}{\partial x}+H\frac{\partial u\prime}{\partial x}=0 \tag{3}$$

Equations (2) and (3) constitute the system for comprehensively understanding ENSO dynamics in this investigation. Note that Eq. (3) can be enclosed by introducing zonal oceanic current anomaly equations just as ZC model had conducted. However, this will further complicate the system and will not be conductive to analytical analysis. Therefore, the system will be enclosed by introducing new approximation relations.

Now let us firstly revisit the approximate relation in constructing the RO model (Jin 1997), that is,

$$\tau\prime=b_1 T\prime \tag{4}$$

where $\tau\prime$ is the zonal wind stress anomaly and b_1 is coupling coefficient. This simple relation between wind stress anomaly and SSTA works since the atmospheric response to a warm SSTA in the central to eastern Pacific is a westerly and the SSTA variable in RO model is averaged over the central to eastern Pacific (Jin 1997). However, this approximation does not work if the SSTA variable is not limited in the central to eastern Pacific as Eq. (2) describes.

According to Gill (1980), the atmospheric response to diabatic heating (which is equivalent to SSTA as Neelin (1989) had pointed out) is a westerly wind west of the heating while an easterly wind east of the heating. Actually, Jin (1997) also pointed out this. He proposed the relation because SSTAs are averaged over the central to eastern Pacific so that the westerly anomaly west of the warm SSTA is the main consideration and also because there is an overall westerly (easterly) anomaly for a positive (negative) SSTA over the entire basin of the equatorial band (e.g., Fig. 1a). To capture the essence of the atmospheric

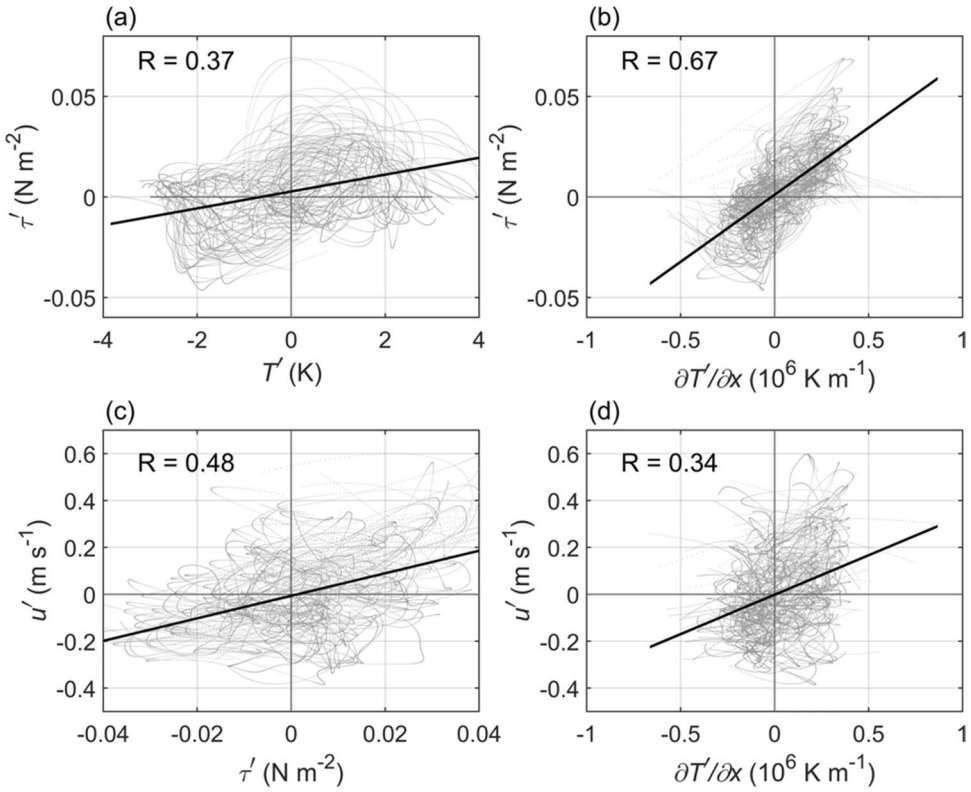

Fig. 1 The linear relations between the SSTA and the zonal wind stress anomaly (**a**), between the gradient of the SSTA and the zonal wind stress anomaly (**b**), between the zonal wind stress anomaly and the oceanic current anomaly (**c**), and between the gradient of the SSTA and the oceanic current anomaly (**d**). The zonally averaged (5°S-5°N mean) monthly anomalies (from January 1980 to December 2020) are selected in the tropical Pacific (150°E-90°W) from months (108 months in total) when the absolute value of the NINO 3.4 index is larger than 1 in the simple ocean data assimilation (SODA) version 3.4.2. All longitude grids (241 in total) are used. Therefore, there are a huge total of 241 × 108 (= 26028) samples. To glorify, the SSTA gradients in (b) and (d) have been amplified 10^6 times as shown in the horizontal labels. All data are spatially smoothed

response to a warm SSTA—westerly (easterly) wind stress anomaly west (east) of a warm SSTA—a new simple relation is proposed here, that is,

$$\tau\prime = b_2 \frac{\partial T\prime}{\partial x} \tag{5}$$

where b_2 is the coupling coefficient. This relation links the wind stress anomaly with the gradient of SSTA. As shown in Fig. 1b, the performance of this approximation relation is better than the relation Eq. (4). Considering the fact that the oceanic current in the mixed layer in general follows the direction of the wind stress (e.g., see Fig. 1c), a simple proportional relation between them may be established, namely,

$$u\prime = b_3 \tau\prime \tag{6}$$

where b_3 is the coefficient. This relation can be further improved by introducing the influence of the thermocline depth anomalies as Jin et al. (2020) suggested.

The above two relations build a linkage between the zonal current anomaly and the gradient of SSTA, that is,

$$u\prime = b \frac{\partial T\prime}{\partial x} \tag{7}$$

where $b = 1.25 \times 10^5 \mathrm{m^2 s^{-1} K^{-1}}$ is the coupling coefficient and is estimated by the linear regression of the gradient of the SSTA data to the oceanic current data in the simple ocean data assimilation (SODA) version 3.4.2 (Carton et al. 2018). The linear relation is enough significant with a correlation coefficient of 0.34 since the value is calculated from a huge total of 26,028 samples. Note that Eq. (7) holds not only for anomalous state but also for the climatological mean state, that is, $\overline{u} = b\frac{\partial \overline{T}}{\partial x}$. This is reasonable since the climatological SST is also associated with the climatological zonal wind stress (Jin and Neelin 1993) and hence the climatological zonal current.

Substituting Eq. (7) into Eq. (3) to eliminate $u\prime$ and replacing the horizontal advection on SST by the anomalous

zonal current, a linear coupled system with both thermocline dynamics and SSTA dynamics may be derived

$$\left(\frac{\partial}{\partial t}+\bar{u}\frac{\partial}{\partial x}\right)T\prime+K_h h\prime=Q\prime \tag{8}$$

$$\left(\frac{\partial}{\partial t}+\bar{u}\frac{\partial}{\partial x}\right)h\prime+Hb\frac{\partial^2 T\prime}{\partial x^2}=0 \tag{9}$$

Note that according to the above analysis, both the thermodynamic and thermocline equations in this investigation can be derived from the classical ZC models (Cane and Zebiak 1985; Cane et al. 1986; Zebiak and Cane 1987). Therefore, the system can be regarded as the simplified version of the ZC model. On the other hand, similar as the classical RO model, the system also contains two variables: SSTA and TDA. Differently, the two variables do not represent the regional mean anomalies, e.g., averaged anomalies in NINO 3 region and over the western Pacific box. They denote the SSTA and TDA in the entire equatorial Pacific and hence having spatial variations. Therefore, it can also be seen as a spatial extension to the classical RO model.

Eliminating $h\prime$ from the system, a wave equation of $T\prime$ may be derived as

$$\left(\frac{\partial}{\partial t}+\bar{u}\frac{\partial}{\partial x}\right)^2 T\prime=c^2\frac{\partial^2 T\prime}{\partial x^2}+\left(\frac{\partial}{\partial t}+\bar{u}\frac{\partial}{\partial x}\right)Q\prime \tag{10}$$

where $c=\sqrt{K_h Hb}=0.25\mathrm{ms}^{-1}$ is the wave speed. Note that although Eq. (10) may demonstrate wave propagation under certain boundary conditions, it is not the equation for the well-known Kelvin or Rossby waves. Actually, the wave speed here can be seen as an indicator of the natural oscillation periods. The oscillation and propagation features will be discussed in the following text.

Introducing the coordinate system that moves with the basic zonal current,

$$x_1=x-\bar{u}t, t_1=t \tag{11}$$

Equation (10) may be further reduced to

$$\frac{\partial^2 T\prime}{\partial t_1^2}=c^2\frac{\partial^2 T\prime}{\partial x_1^2}+\frac{\partial Q\prime}{\partial t_1} \tag{12}$$

Equation (12) is a standard wave equation and is easier to solve.

3 The solution

To make the deriving process simpler and clearer, the solution for Eq. (12) is derived and presented below. After the solution is obtained, it will be easy to write the solution for Eq. (10) according to the coordinate transform Eq. (11).

The initial values are specified as

$$T\prime(x_1)\big|_{t_1=0}\equiv F(x_1) \tag{13}$$

$$h\prime(x_1)\big|_{t_1=0}\equiv G(x_1) \tag{14}$$

where $F(x_1)$ and $G(x_1)$ are known functions. The well-posed free boundary conditions are specified as

$$\frac{\partial T\prime}{\partial x_1}\bigg|_{x_1=0}=0,\ \frac{\partial T\prime}{\partial x_1}\bigg|_{x_1=L}=0 \tag{15}$$

where L is the basin width of the equatorial Pacific. Expanding $T\prime$ and $Q\prime$ into cosine series, e.g.,

$$\{T\prime,Q\prime\}=\sum_{n=0}^{\infty}\{T_n(t_1),Q_n(t_1)\}\cos(\lambda_n x_1) \tag{16}$$

where $\lambda_n=\frac{n\pi}{L}$, will naturally satisfy the boundary conditions Eq. (15). Similarly, $F(x_1)$ and $G(x_1)$ are also expanded as cosine series,

$$\begin{Bmatrix}F(x_1)\\G(x_1)\end{Bmatrix}\equiv\begin{Bmatrix}T\prime(x_1)\\h\prime(x_1)\end{Bmatrix}\bigg|_{t_1=0}=\sum_{n=0}^{\infty}\begin{Bmatrix}T_n(0)\\h_n(0)\end{Bmatrix}\cos(\lambda_n x_1)\equiv\sum_{n=0}^{\infty}\begin{Bmatrix}f_n\\g_n\end{Bmatrix}\cos(\lambda_n x_1) \tag{17}$$

It is easy to derive a second-order differential equation with constant coefficients by substituting these cosine series into Eq. (12), that is,

$$\frac{d^2 T_n}{dt_1^2}+\omega_n^2 T_n=\frac{dQ_n}{dt_1} \tag{18}$$

where $\omega_n=c\lambda_n$. When $n=1,2,3,\cdots$, the solution for Eq. (18) is

$$T_n(t_1)=A_n\cos(\omega_n t_1)+B_n\sin(\omega_n t_1)+\frac{1}{\omega_n}\int_0^{t_1}\frac{dQ_n}{d\tau}\sin\omega_n(t_1-\tau)d\tau \tag{19}$$

where $A_n=f_n, B_n=\frac{q_n-K_h g_n}{\omega_n}, q_n=Q_n(0)$ are coefficients that are determined by initial values. Equation (18) indicates a forced oscillation. Its free oscillation part is formally the same as the harmonic oscillation in the original RO model (Jin 1997). It is obvious that Eq. (18) further extends the RO model to associate with spatial modes. Or, the original RO

model only reflects the oscillation of a specified spatial mode. In this sense, it may be regarded as a spatial RO model.

When $n = 0$, Eq. (18) becomes

$$\frac{d^2T_0}{dt_1^{\,2}} = \frac{dQ_0}{dt_1} \tag{20}$$

and the solution is

$$T_0(t_1) = A_0 + B_0 t_1 + \int_0^{t_1} Q_0(\tau)d\tau \tag{21}$$

where $A_0 = f_0$, $B_0 = 0$ are coefficients. Note that B_0 should be zero to make sure SSTA is limited when time is long enough. A_0 is a constant value that is determined by initial SSTA values. $\int_0^{t_1} Q_0(\tau)d\tau$ is a time-related term that relies on the integral of the constant term in cosine series of the net surface heating. Note that there is no spatial variation when $n = 0$. Therefore, this solution denotes a basin-wide consistent variation mode.

The solution for Eq. (12) can be eventually expresses as

$$\begin{aligned} T\prime(x_1,t_1) &= f_0 + \textstyle\int_0^{t_1} Q_0(\tau)d\tau \\ &+ \textstyle\sum_{n=1}^{\infty}\left[f_n\cos(\omega_n t_1) + \frac{q_n - K_h g_n}{\omega_n}\sin(\omega_n t_1)\right]\cos(\lambda_n x_1) \\ &+ \textstyle\sum_{n=1}^{\infty}\frac{1}{\omega_n}\left[\int_0^{t_1}\frac{dQ_n}{d\tau}\sin\omega_n(t_1-\tau)d\tau\right]\cos(\lambda_n x_1) \end{aligned} \tag{22}$$

or

$$\begin{aligned} T\prime(x_1,t_1) &= f_0 + \textstyle\int_0^{t_1} Q_0(\tau)d\tau + \sum_{n=1}^{\infty} C_n\sin(\omega_n t_1 + \theta_n)\cos(\lambda_n x_1) \\ &+ \textstyle\sum_{n=1}^{\infty}\frac{1}{\omega_n}\left[\int_0^{t_1}\frac{dQ_n}{d\tau}\sin\omega_n(t_1-\tau)d\tau\right]\cos(\lambda_n x_1) \end{aligned} \tag{23}$$

where $C_n = \sqrt{f_n^2 + \left(\frac{q_n - K_h g_n}{\omega_n}\right)^2}$ is the amplitude, θ_n is the phase, and $\sin\theta_n = \frac{f_n}{C_n}$, $\cos\theta_n = \frac{q_n - K_h g_n}{C_n\omega_n}$. Equation (22) or Eq. (23) demonstrates that the spatiotemporal variation of SSTA can be decomposed into the summation of a series of spatial modes, each of which oscillates with a natural frequency of ω_n and a forced frequency.

For a specific spatial mode (ignoring the net surface heating), each point of the spatial mode oscillates with its natural frequency and with the same phase but varying amplitude of $\left|C_n\cos\lambda_n x_1\right|$ that depends on its location in the spatial mode. This can also be called a stationary wave with zero phase speed. In other words, this specific spatial mode ($\cos\lambda_n x_1$) oscillates with a natural frequency ω_n, a phase θ_n, and an amplitude C_n. The temporal variation will become more complex when considering the effect of the net surface heating forcing which may add at least one external forced frequency to the natural frequency for the specific spatial mode. Particularly, if a forced frequency is just right equal to the natural frequency, the corresponding amplitude will tend to be infinity due to resonance. Specific calculation cases will be given in the next section.

Transforming to the (x, t) coordinate system, Eq. (23) becomes

$$\begin{aligned} T\prime(x,t) &= f_0 + \textstyle\int_0^{t} Q_0(\tau)d\tau + \sum_{n=1}^{\infty} C_n\sin(\omega_n t + \theta_n)\cos\lambda_n(x - \bar{u}t) \\ &+ \textstyle\sum_{n=1}^{\infty}\frac{1}{\omega_n}\left[\int_0^{t}\frac{dQ_n}{d\tau}\sin\omega_n(t-\tau)d\tau\right]\cos\lambda_n(x - \bar{u}t) \end{aligned} \tag{24}$$

Since $\cos\lambda_n(x - \bar{u}t) = \cos\lambda_n x\cos\bar{u}t + \sin\lambda_n x\sin\bar{u}t$, Eq. (24) becomes

$$\begin{aligned} T\prime(x,t) &= f_0 + \textstyle\int_0^{t} Q_0(\tau)d\tau \\ &+ \textstyle\sum_{n=1}^{\infty} C_n\left[\sin(\omega_n t + \theta_n)\cos\bar{u}t\right]\cos\lambda_n x \\ &+ \textstyle\sum_{n=1}^{\infty}\frac{1}{\omega_n}\left[\cos\bar{u}t\int_0^{t}\frac{dQn}{d\tau}\sin\omega_n(t-\tau)d\tau\right]\cos\lambda_n x \\ &+ \textstyle\sum_{n=1}^{\infty} C_n\left[\sin(\omega_n t + \theta_n)\sin\bar{u}t\right]\sin\lambda_n x \\ &+ \textstyle\sum_{n=1}^{\infty}\frac{1}{\omega_n}\left[\sin\bar{u}t\int_0^{t}\frac{dQn}{d\tau}\sin\omega_n(t-\tau)d\tau\right]\sin\lambda_n x \end{aligned} \tag{25}$$

The last two terms in Eq. (25) represent temporal variations associating with spatial modes of sine curves. It is obvious that the different locations in the basin will have different phases due to modulation of the sine and cosine spatial modes. In other words, Eq. (25) may manifest traveling waves. Equation (25) is equivalent to the solution of Cauchy problem for Eq. (10) with no specified boundary conditions. It means that SSTA perturbations may propagate across the coastlines as if the coastlines do not exist. However, considering the fact that waves may be reflected or absorbed due to the blocking effect of the coastlines, Eq. (25) may be applied to analyze the wave propagation toward a far distant coastline so that the influence of the boundary can be ignored. This limitation comes from the practice that specifies a basin-wide constant zonal basic current that should have been zero at the coastlines. The constant zonal basic current over the entire basin means that it is hard to specify well-posed boundary conditions at the coastlines. Therefore, a spatial varying zonal basic current that vanishes at the coastlines seems a better choice. Besides, an external frequency that associates with the zonal basic current is added on the temporal oscillations. Generally speaking, the zonal basic current further complicates the solution in both spatial and temporal dimensions.

4 Results

To provide a fundamental scene for understanding the spatiotemporal oscillator model, the results are provided based on Eq. (23). It is equivalent to moving with the zonal basic

current or ignoring the basic zonal current for easy understanding. The first spatial mode ($n = 1$) is a standard cosine curve in the $[0, L]$ range with a period of 2π, hence a SSTA pattern with warm (or cold) SSTA in the western Pacific but cold (or warm) SSTA in the eastern Pacific. The second spatial mode ($n = 2$) is a standard cosine in the $[0, L]$ range with a period of π, hence a SSTA pattern with cold (or warm) SSTA in the central Pacific but warm (or cold) SSTA in the eastern and western Pacific. These two spatial patterns can be seen as the theoretical prototype of the EP and CP El Niño events. Note that even if the first two modes are similar to the EP and CP El Niño events, they are not the observed EP and CP El Niño events. Actually, an EP or CP El Niño event should be seen as the combination of different modes with different weights. For higher-order modes, SSTA patterns associate with small-scale structures and do not have clear physical images so far. Therefore, only the first two spatial modes are used.

4.1 Natural oscillation

To highlight the first two natural spatiotemporal oscillation modes, their expressions are written separately,

$$T_n = \sin\left(\omega_n t_1 + \frac{\pi}{2}\right)\cos\left(\lambda_n x_1\right) \tag{26}$$

where $n = 1, 2$. The initial phases are set to be $\frac{\pi}{2}$, denoting that the SSTA in each mode has the maximum value while the TDA equals zero at the beginning time. They are also summed with different weights to highlight their relative importance in constructing SSTA patterns, that is,

$$T\prime = 2T_1 + T_2 \tag{27}$$

and

$$T\prime = T_1 + 2T_2 \tag{28}$$

For the first mode ($n = 1$), SSTA in the eastern and western Pacific (Fig. 2a) oscillates with alternative warm and cold anomalies and with a natural period of $\mathrm{T}_1 = \frac{2L}{c} \approx 4.6$ years. For the second mode ($n = 2$), SSTA (Fig. 2b), with warm anomalies appearing in the central Pacific while cold anomalies in the western and eastern Pacific, oscillates with a natural period that is half of the first mode, that is, $\mathrm{T}_2 = \frac{L}{c} \approx 2.3$ years. It is interesting to point out that these two natural periods are consistent with the previous studies that suggested the EP and CP El Niño events oscillate with QQ and QB modes (Bejarano and Jin 2008; Ren and Jin 2013; Xie and Jin 2018). However, these two modes are the physical decomposition of spatiotemporal SSTA variations. They denote the natural oscillations of the system. This is different from the eigenvector analysis that is based on a modified linearized ZC model (Bejarano and Jin 2008; Xie and Jin 2018) and also different from the statistical analysis that is based on observation and reanalysis data (Ren et al. 2013). On the other hand, since both the thermodynamic and thermocline dynamic equations this investigation applied can be derived from the commonly applied ZC model, this spatiotemporal oscillator model is actually the

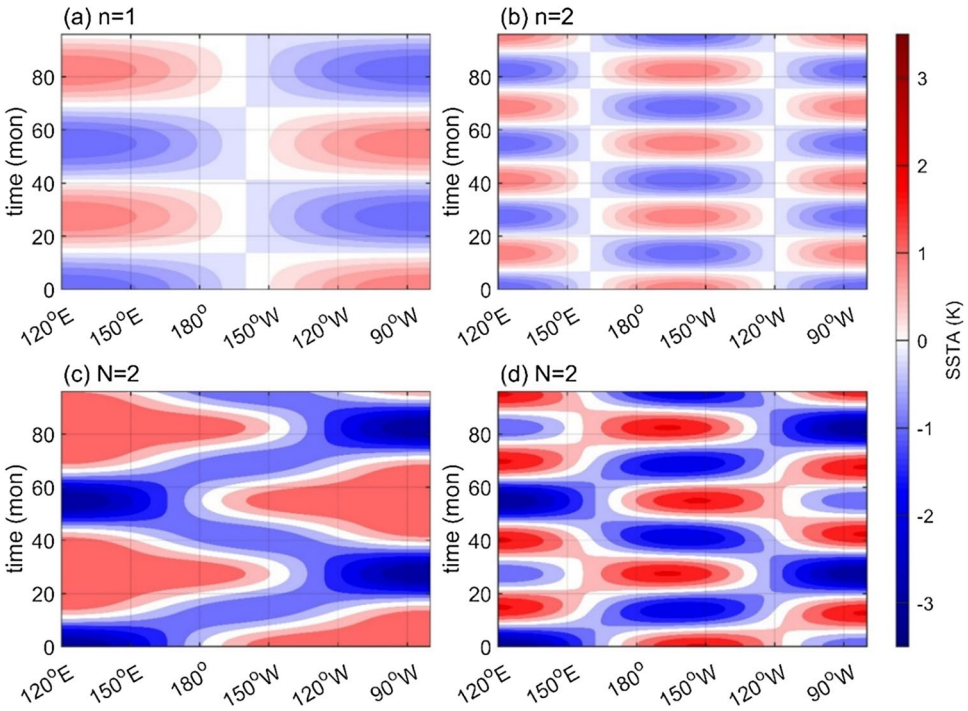

Fig. 2 The temporal evolution for the first mode (**a**), the second mode (**b**), the combination of them as Eq. (27) declares (**c**), and as Eq. (28) declares (**d**)

physical simplification to the ZC model. Therefore, the two natural oscillation modes can also be seen as a theoretical explanation for previous studies.

If the first mode is more dominant, the warm SSTA in the eastern Pacific can extend from 80°W to around 180° at the beginning time (Fig. 2c), larger than the warm SSTA in the first mode where the warm and cold anomalies halve the equatorial Pacific. On the other hand, the cold SSTA in the eastern Pacific shrinks to 140°W–80°W range. The SSTA pattern in this combination looks quite similar to the SSTA pattern in the strong El Niño events, such as in 1982/83, 1997/98, and 2015/16, in which warm SSTAs appear in the central to eastern Pacific. It implies that these strong El Niño events may rely on the coordination between the two modes. On the other hand, if the second mode is more dominant, the warm SSTA still locates in the central Pacific at the beginning time (Fig. 2d), that is quite similar to case for the second mode alone (Fig. 2b). The variation in the spatial pattern shows the regulation effect of the first mode is relatively minor in the CP El Niño events. Note that the dipolar and tripolar SSTA structures look a little different from the observed patterns. For instance, CP El Niño events display a dipolar pattern with negative SSTA in the western Pacific while positive SSTA extending from the central to eastern Pacific, albeit with a central Pacific center of action (Kug et al. 2009). This discrepancy is caused by the fact that only the first two modes are taken into consideration. As pointed out previously, the first and the second modes only represent the natural dipolar and tripolar SSTA oscillations in the tropical Pacific, or the QQ and QB modes, respectively. However, the specific SSTA pattern in an El Niño event is the superposition of different modes with different weights. For example, the relative weak cool SSTA in the western Pacific and a strong warm SSTA in the eastern Pacific suggest that there is a basin-wide warming mode (corresponding to $n = 0$). Therefore, we may estimate that the tripolar SSTA pattern will move upward as a whole if considering the basin-wide warming mode. This will amplify the positive SSTA in the central Pacific while shrink the negative SSTA in the eastern Pacific (even changing to a weak positive SSTA). It is obvious that this will make the tripolar pattern closer to the observational results and even much closer to the observations if more natural spatial modes are introduced.

According to Eq. (26), the first two modes of TDA variation can be written as

$$h_n = -\frac{1}{K_h}\frac{\partial T_n}{\partial t} = -\frac{\omega_n}{K_h}\cos\left(\omega_n t_1 + \frac{\pi}{2}\right)\cos\left(\lambda_n x_1\right) \tag{29}$$

Equation (29) denotes that TDA variations have the same spatial pattern as SSTA variations but with a phase lag in the temporal variations. Therefore, the temporal evolution for the different modes of TDA is not portrayed. According to Eq. (29), the amplitude of each mode is proportional to the natural frequency. The faster the natural frequency is (equivalent to larger expansion order n), the larger the amplitude is. This is quite different from the SSTA modes. Of course, the amplitude will become smaller and smaller with increasing expansion order n due to limited variations in observed TDA.

The time series of NINO 3.4 index and the box mean TDA in NINO 3.4 region (Fig. 3) are further portrayed to

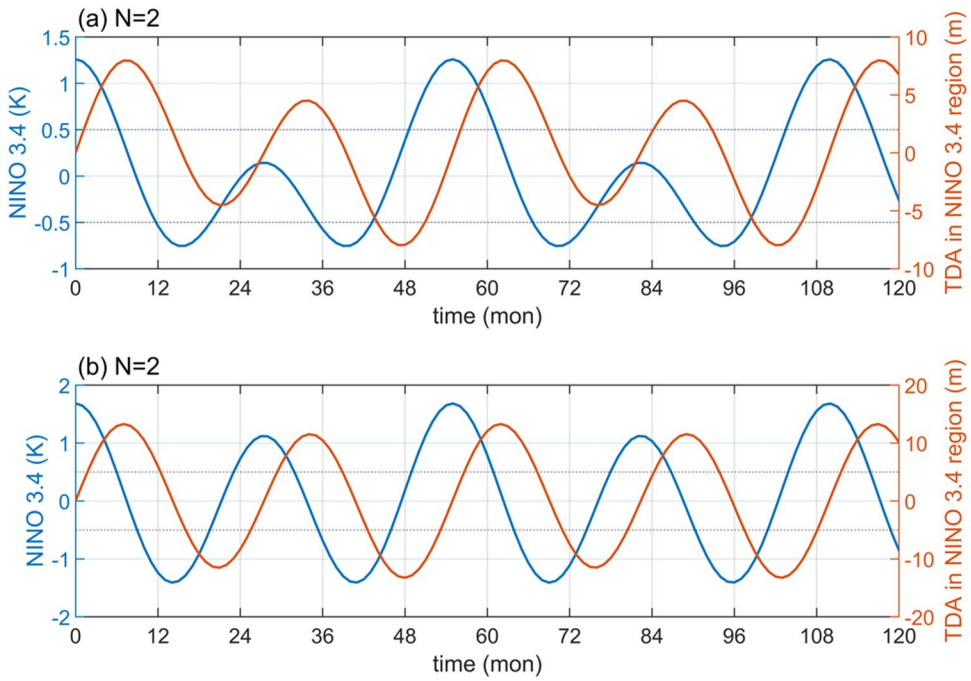

Fig. 3 The variations in NINO 3.4 index and box mean TDA in NINO 3.4 region for the combinations of the two modes as shown in Fig. 2c, d

demonstrate the temporal variations. For the case in which the first spatial mode is more dominant as Eq. (27) exhibits, NINO 3.4 index (Fig. 3a) decreases from a maximum value of around 1.2 K to − 0.7 K within around 13 months and then increases to an extreme value of around 0.1 K within around 27 months to finish a cycle, the natural period of the second mode. Within the next 27 months, it moves to the same minimum value and then the maximum value to form a larger period of 54 months, the natural period of the first mode. If an El Niño event is defined by NINO 3.4 index that is larger than 0.5 K while La Niña event by the index smaller than − 0.5 K, it is quite interesting to find that two La Niña events will follow an El Niño event. For the case that the second spatial mode is more dominant as Eq. (28) shows, NINO 3.4 index (Fig. 3b) has the similar variation trend as the case that the first mode is more dominant but with different amplitudes. NINO 3.4 index is larger than 0.5 K (or around 1 K) near the 27th month so that an El Niño event can be defined, which blocks the two La Niña events in a row as they occurred successively in the previous case. Therefore, El Niño and La Niña events happen alternatively in this case. In both two cases, TDA index has the same temporal variations as the NINO 3.4 index but with a phase lag. Besides, the intensity of two adjacent El Niño events is also different. It is obvious that the situation will be more complex if considering different combination weights and different initial phases. This is right the capacity of the model for understanding ENSO STPD.

4.2 Forced oscillation

To consider the effect of the net surface heat flux forcing, cosine expansion is conducted for the 5°S–5°N mean equatorial Pacific net surface heat flux anomaly in the SODA version 3.4.2 data. Spectrum analysis suggests that the first spatial mode has a most significant annual oscillation with a period of 12 months (Fig. 4a), while the second spatial mode has a significant decadal oscillation with a period of around 114 months (Fig. 4b). Therefore, these two significant periods are added and are analytically expressed as

$$Q_n = \overline{Q}_0 \cos\left(\widehat{\omega}_n t_1\right) \cos\left(\lambda_n x_1\right) \tag{30}$$

where $n = 1, 2$, $\widehat{\omega}_1 = \frac{2\pi}{12}\text{month}^{-1}$ represents the significant annual cycle for the first spatial mode, $\widehat{\omega}_2 = \frac{2\pi}{114}\text{month}^{-1}$ denotes the significant decadal oscillation (around 9.5 years) for the second spatial mode, and $\overline{Q}_0 = 4.89 \times 10^{-8} Ks^{-1}$ equivalent to a relatively weak net surface heating flux of $10 Wm^{-2}$. According to Eqs. (23) and (26), SSTA variations for the first and second modes are

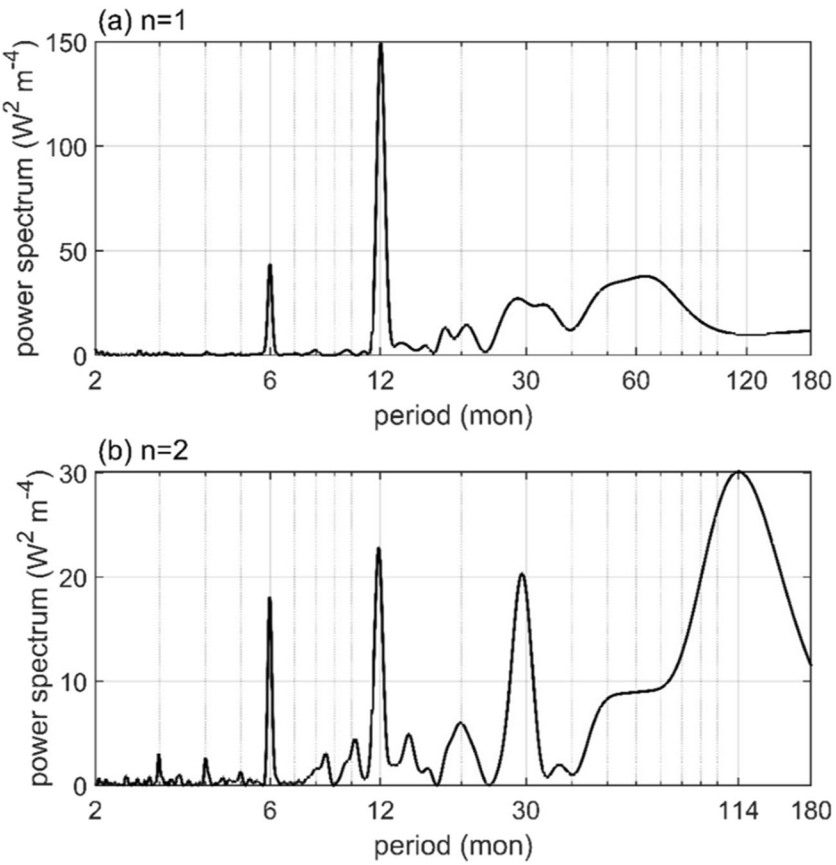

Fig. 4 The power spectrum of the time series for the first two spatial modes of the net surface heating

$$T_n(x_1,t_1)=\left[\sin\left(\omega_n t_1+\frac{\pi}{2}\right)-\frac{\widehat{\omega}_n}{\omega_n}\int_0^{t_1}\sin\widehat{\omega}_n\tau\sin\omega_n(t_1-\tau)d\tau\right]\cos(\lambda_n x_1)=\left[\sin\left(\omega_n t_1+\frac{\pi}{2}\right)-\frac{\widehat{\omega}_n}{\omega_n}\frac{1}{\widehat{\omega}_n^2-\omega_n^2}\left(\widehat{\omega}_n\sin\omega_n t_1-\omega_n\sin\widehat{\omega}_n t_1\right)\right]\cos(\lambda_n x_1) \quad (31)$$

The forced oscillations (Fig. 5) are basically the same as the previous natural oscillations (Fig. 2). For the first mode ($n = 1$), except for the significant period of around 4.6 years, the SSTA (Fig. 5a) also oscillates with the forced period of 1 year (annual cycle) even though its modulation on SSTA is relatively minor due to relative weak intensity of the net surface heating. For the second mode ($n = 2$), the situation is similar. It also oscillates with a natural period and a forced period. Similar to previous subsection, the two modes in Eq. (31) are also combined with different weights as Eqs. (27) and (28) suggest. For the case that the first mode is more dominant, the warm SSTA pattern (Fig. 5c) also looks similar to the EP El Niño events but with significant difference with the previous natural case. For example, the warm SSTA has a largest spatial range at the beginning. It gradually shrinks to the eastern Pacific but with strengthening intensity. After the amplitude of SSTA arrives the peak, it will quickly weaken to become a strong La Niña event, which will have matched intensity and spatial range as the El Niño event. The time series of NINO 3.4 index (Fig. 6a) oscillates with two significant periods of 4.6 and 2.3 years—the natural periods of the first two modes. Although the forced period is not significant and cannot be seen directly in Fig. 6a, it indeed exhibits its influence on complicating the time series to make one short period cycle slightly different from the other. For the case that the second mode is more dominant, the variations in SSTA pattern (Fig. 5d) are quite similar to that in the previous natural case. Modulated by the natural periods and the forced period, the time series of NINO 3.4 index (Fig. 6b) also becomes more complex. It is interesting to point out that observations also reveal decadal oscillation in central Pacific SST (e.g., Power et al. (2021)). A simple model suggests that decadal variability can be explained by random changes in the relative number and magnitude of La Niña and El Niño events from decadal to decadal (Power and Colman 2006). Furthermore, other factors, such as the Pacific subtropical cells (Capotondi et al. 2005), the greenhouse gas emission (Xie et al. 2010), and the nonlinear dynamical heating (Liu et al. 2022), have also been used to explain some decadal variability in the Pacific Ocean. Here in this investigation, a decadal signal from the net surface heating can also force corresponding decadal variability in the Pacific Ocean. Further studies may promote the understanding of the decadal variability. Note that the first and second spatial modes for the net surface heating also have significant periods of around 60 and 30 months (see Fig. 4) that are close to the corresponding natural periods. And if these two forced periods are specified in Eq. (30),

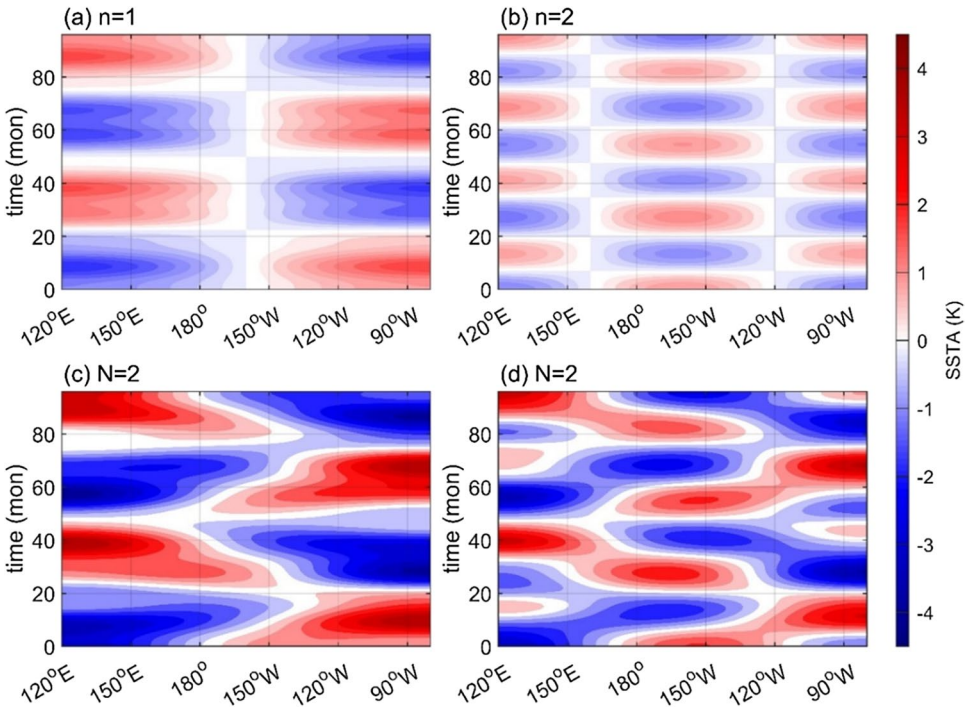

Fig. 5 The same as Fig. 2, but for the forced oscillation

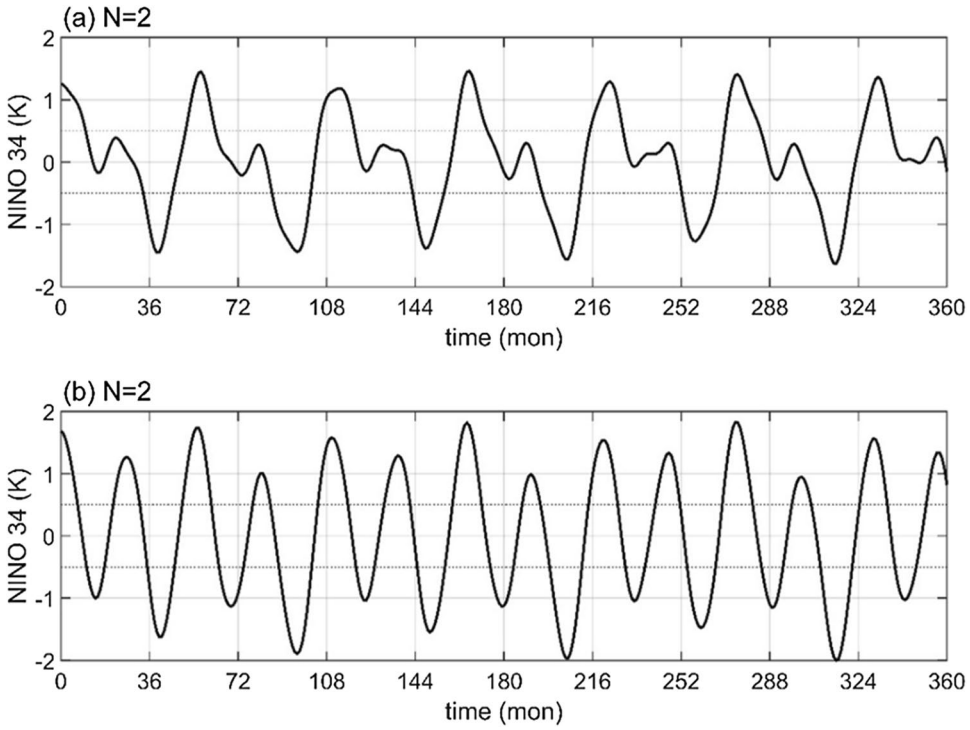

Fig. 6 The same as Fig. 3, but only for the forced oscillation in NINO 3.4 index

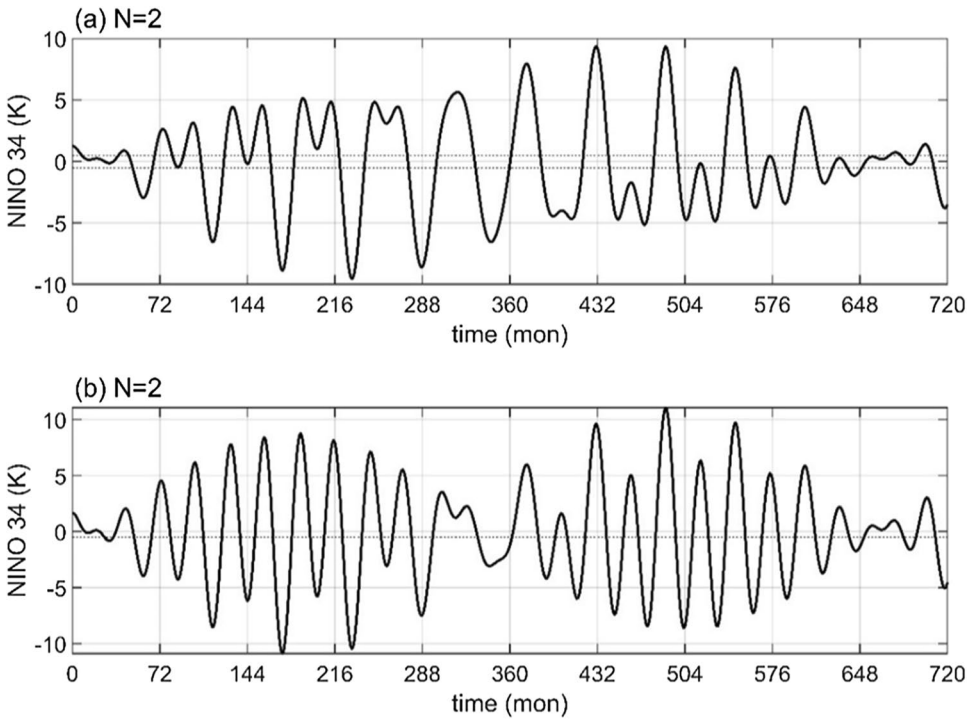

Fig. 7 The same as Fig. 6, but the forced periods are set to 60 and 30 months for the first and second modes, respectively

they will induce resonance to produce unreasonable strong NINO 3.4 index oscillation as Fig. 7 exhibits. During a certain time period, a forced frequency may be close to a natural frequency. This may breed significant SSTA variations that may be provide a plausible explanation for strong ENSO events in this time period.

5 Discussions

5.1 The relation between the SSTAs and the wind stress anomalies

Equation (5) characterizes the symmetric westerly and eastly wind stress anomalies on the west and east sides of a warm SSTA. However, this simple relation may be a little rough to capture the relatively weak easterly anomalies on the east side of the warm SSTA. Since the wind stress anomalies are closely linked with the SSTA and its gradient (see Fig. 1a, b), an improved simple relation may be proposed by combining Eqs. (4) and (5), that is,

$$\tau\prime = b_3 T\prime + b_4 \frac{\partial T\prime}{\partial x} \tag{32}$$

where b_3 and b_4 are coupling coefficients. This relation may also be found in the classical paper of Gill (1980), in which the zonal wind stress anomaly is analytically expressed as a function of the heating and its gradient (e.g., see Gill's Eqs. (4.2) and (4.3) in his paper). Equation (32) can improve the statistical relationship among SSTA, the gradient of SSTA, and the zonal wind stress anomaly (Fig. 8a) and increase the correlation coefficient to 0.69. Based on this relation, Eq. (7) becomes

$$u\prime = b_5 T\prime + b_6 \frac{\partial T\prime}{\partial x} \tag{33}$$

where $b_5 = 0.0446\text{ms}^{-1}\text{K}^{-1}$ and $b_6 = 8.1137 \times 10^4\text{m}^2\text{s}^{-1}\text{K}^{-1}$ are coupling coefficients that are determined from the SODA version 3.4.2 data. Equation (33) also improves the relation among SSTA, the gradient of SSTA, and the surface oceanic current anomaly (Fig. 8b). The correlation coefficient now becomes 0.47.

With this improved relation, Eq. (12) becomes

$$\frac{\partial^2 T\prime}{\partial t_1^2} = a\frac{\partial T\prime}{\partial x_1} + c^2\frac{\partial^2 T\prime}{\partial x_1^2} + \frac{\partial Q\prime}{\partial t_1} \tag{34}$$

where $a = K_h H b_5 \approx 2.23 \times 10^{-8}\text{ms}^{-2}$ and $c = \sqrt{K_h H b_6} \approx 0.20\text{ms}^{-1}$ have dimensions of acceleration and velocity, respectively. It is easy to introduce $T\prime = \widehat{T}e^{-\sigma x_1}$ and $Q\prime = \widehat{Q}e^{-\sigma x_1}$ where $\sigma = \frac{a}{2c^2}$ to reduce Eq. (34) to a standard form,

$$\frac{\partial^2 \widehat{T}}{\partial t_1^2} = c^2\frac{\partial^2 \widehat{T}}{\partial x_1^2} - \mu^2\widehat{T} + \frac{\partial \widehat{Q}}{\partial t_1} \tag{35}$$

where $\mu^2 = \frac{a^2}{4c^2}$. It has the same form as Eq. (12) except for an additional $-\mu^2\widehat{T}$ term and it is also easy to derive its analytic solution by expanding $\widehat{T}$ to cosine series as before. Substituting the cosine series expansion solution into Eq. (35), we can derive

$$\frac{d^2 T_n}{dt_1{}^2} + \varpi_n^2 T_n = \frac{dQ_n}{dt_1} \tag{36}$$

where $\varpi_n^2 = \omega_n^2 + \mu^2$, $n = 0, 1, 2, \cdots$. It has the same form as Eq. (18) but with modified natural frequencies. Therefore, the influence of the new introduced parameter will be only discussed. Note that the natural frequency will be modified by the parameter μ and hence a with no simple multiple relation. For example, the first natural period ($n = 1$) becomes around 3 years, while the second natural period ($n = 2$) becomes around 2.2 years. Besides, there will exist a new zeroth-order ($n = 0$) natural period of around 3.6 years (the corresponding natural frequency equals μ), that is, close to the first-order natural period. In addition to variations in temporal oscillations, the spatial modes are also modified by the factor $e^{-\sigma x_1}$. Nonetheless, the theoretical framework is still the same and no explicit explanation of this solution is provided in present investigation. This can be done in the near future.

5.2 Propagation feature

According to Eq. (23), an observer who moves with the zonal basic current (or an stationary observer due to zero zonal

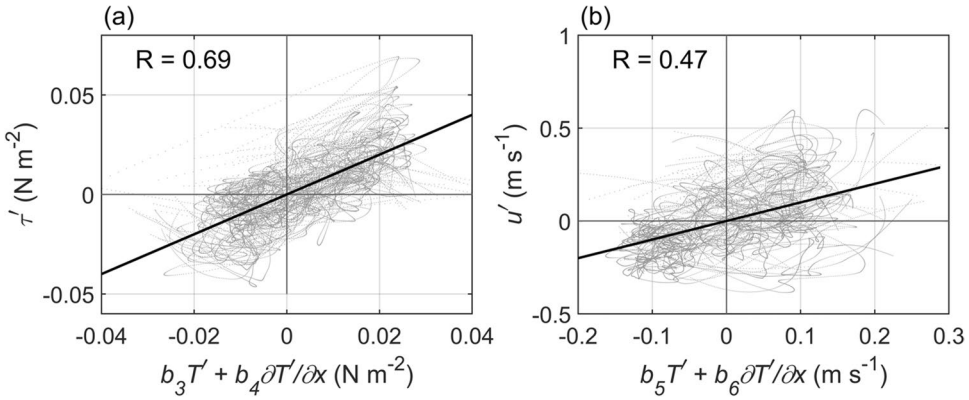

Fig. 8 The linear relations between the combination of SSTA and its gradient and the zonal wind stress anomaly (**a**) and the oceanic current anomaly (**b**). The data come from the SODA version 3.4.2. The detailed information is the same as Fig. 1

basic current) will see SSTA oscillation with no propagation. However, as Eq. (25) suggests, he or she may still observe wave propagation if the blocking effect of the boundary is too weak to be ignored. This works when a perturbation propagates toward a distant coastline. Besides, if the initial perturbation (the initial value) is only significant in a local region (e.g., in coastal regions) rather than the entire basin, the mutual interaction region between the westward propagating and eastward propagating waves will be near the initial region. This means that a region, if it is far away from the initial perturbation, is only influenced by the westward or the eastward propagating wave. Therefore, at the place that is far away from the initial field, Eq. (12) can be described by a simple westward propagating equation and a simple eastward propagating equation,

$$\frac{\partial T\prime}{\partial t_1} - c\frac{\partial T\prime}{\partial x_1} = 0 \tag{37}$$

$$\frac{\partial T\prime}{\partial t_1} + c\frac{\partial T\prime}{\partial x_1} = 0 \tag{38}$$

Note that the net surface heating has been ignored here. Particularly, if the initial values only dominate near the western or eastern coastal region, Eq. (12) can be replaced by Eq. (37) or Eq. (38) to highlight the eastward or westward propagating wave, that should be most significant in the central Pacific that is both far away from the initial perturbation and far away from the coastlines. When the propagating wave is closing to the coastline, it may be absorbed or reflected by the coastline.

For some cases the eastern coastal SSTA may play roles, westward propagating waves may be observed. For example, Horel (1982) had pointed out that relatively warm SST appears in December–January along the coast of Peru and then spreads westward along the equator during the next several months. This propagating speed is around -0.5 m s^{-1} (Boucharel et al. 2013) and is basically in agreement with the wave propagation speed $\overline{u} - c = -0.35ms^{-1}$ (setting $\overline{u} = -0.1ms^{-1}$). Considering the fact that the zonal basic current in the eastern Pacific is generally larger than 0.1 m s^{-1} (Keenlyside and Kleeman 2002), the theoretical propagation speed will be further closer to the observational propagation speed. For some cases the influence of the western Pacific SSTA may be more significant. Therefore, eastward propagating waves may be observed. For example, Simon Wang et al. (2015) found a systematic propagating pattern of SSTA has emerged between 100°E and 160°W, linking warm (cold) water in the western North Pacific to the development of El Niño (La Niña) in the central equatorial Pacific, for a duration of about 2–3 years. The corresponding propagation speed is about 0.1–0.16 m s^{-1}, quite consistent with the eastward propagating speed $\overline{u} + c = 0.15ms^{-1}$.

The dispersion relation of the propagating waves can also be discussed by specifying the single wave solution, e.g., $T\prime \sim T_k expi(kx - \omega t)$, $Q\prime \sim Q_k expi(kx - \omega t)$, where k is the wavenumber, ω is the frequency, and T_k and Q_k are corresponding coefficients. Substituting them into Eq. (12) or Eq. (10), the dispersion relation is derived as

$$\omega\prime^2 - i\alpha_k\omega\prime - c^2k^2 = 0 \tag{39}$$

where $\omega\prime = \omega - \overline{u}k$ is the intrinsic frequency and $\alpha_k = Q_k/T_k$ is the ratio between the coefficients. Equation (39) is a quadratic equation but with complex coefficients. It means the frequency will be complex, e.g., $\omega = \omega_r + i\omega_i$, where ω_r and ω_i are real values. Dividing it into real and imagery parts, it becomes

$$\begin{aligned} \omega_r &= \overline{u}k \pm \sqrt{c^2k^2 - \tfrac{1}{4}\alpha_k^2} \\ \omega_i &= \tfrac{1}{2}\alpha_k \end{aligned} \tag{40}$$

The first equation in Eq. (40) demonstrates a propagating wave with energy dispersion. It is obvious that the net surface heating will modulate the wave frequency. The second equation in Eq. (40) means that the wave will develop to be unstable if $\alpha_k > 0$ but will decay if $\alpha_k < 0$. The net surface heating in the equatorial Pacific generally acts on the thermodynamic damping (Jin et al. 2020). Therefore, we may generally set $\alpha_k < 0$. The dependence of α_k on the spatial scale (or the wavenumber) means waves with different spatial scales will have different decay rates. Besides, although α_k is generally smaller than zero, it may be larger than zero for specific wavenumbers in certain cases. This implies that the corresponding waves will be unstable. If the net surface heating is replaced by a Newtonian cooling coefficient α for simplicity in Eq. (1), it is equivalent to set $\alpha_k = -\alpha < 0$ in Eq. (39). This results the waves, no matter what the wavenumbers are specified, will have a constant decline rate that equals half the Newtonian cooling coefficient. Particularly, if neglecting the net surface heating force, Eq. (39) can be reduced to a neutral wave with no energy dispersion,

$$\omega = \omega_r = \left(\overline{u} \pm c\right)k \tag{41}$$

6 Conclusions

A new model is built to capture the essence of the spatiotemporal variations of the ENSO phenomenon in this study. The model contains two variables, SSTA and TDA. The equation for SSTA considers the horizontal advection, the thermocline feedback process, and the net surface heating. The equation for TDA takes the horizontal advection and the divergence of the zonal current anomaly into consideration.

Both equations can be derived from those in the ZC models and therefore can be thought a simplified version of the ZC model. To benefit theoretical analysis, the zonal current anomalies are supposed to be proportional to the zonal wind stress anomalies based on the fact that the oceanic current in the mixed layer is mainly driven by the wind stress. Then the zonal wind stress anomalies are hypothesized to be proportional to the gradients in SSTAs, rather than SSTAs themselves as in the classical RO framework. Of course, a more precise hypothesis that emphasizes the linkage among the zonal wind stress anomalies, SSTAs, and gradients in SSTAs can also be proposed. With above two steps, a proportional relationship between the zonal current anomalies and the gradients in SSTAs is established to enclose the system to a wave equation for SSTAs.

With initial values and proper boundary conditions, the analytic solution is derived by applying cosine series expansion to separate the temporal and spatial variations of SSTA. The solution demonstrates that SSTA variations can be decomposed into the superposition of a series of spatial modes that oscillate with both natural frequencies and forced frequencies. The first spatial mode highlights SSTA contrast between the eastern and western Pacific. The warm (or cold) SSTAs appear in the eastern Pacific while cold (or warm) SSTAs are in the western Pacific. Ignoring the external forcing, it oscillates with a natural period of around 4.6 years. The spatial pattern of the first mode is the theoretical prototype of the EP El Niño events and its natural period is also consistent with the QQ mode. The second spatial mode emphasizes SSTA contrast between the central and eastern, western Pacific. The warm (or cold) SSTAs are located in the central Pacific while the cold (or warm) SSTAs are in the eastern and western Pacific. It oscillates with a natural period of around 2.3 year, the half of the first natural period. The spatial pattern of the second mode is the theoretical prototype of the CP El Niño events and its natural period is also quite consistent with the QB mode. Therefore, the first two modes can provide an explicit physical image of the spatial patterns of two types of ENSO and their temporal variations. Adding these two eigenmodes together with different weights, they may characterize SSTA patterns in the strong El Niño events (e.g., twice the first plus the second) and SSTA patterns in the CP El Niño-like events (e.g., twice the second plus the first). The combined SSTA patterns show complex temporal variations. For example, two La Niña events may alternatively appear after an El Niño event if observing from the NINO 3.4 index. This may be enlightening for understanding the Triple Niña events that happened during in past 3 years (note that they had also appeared before) if considering more eigenmodes.

The net surface heating will exert its influence by introducing forced frequencies. Cosine series expansion for the net surface heating in SODA suggests that there exist many significant oscillation periods, such as 6 and 12 months for the first spatial mode, and 6, 12, 30, and 114 months for the second spatial mode. It is obvious that these forcing periods will modulate natural periods to further complicate the temporal variations. Particularly, if the forcing period is close to the natural period, resonance will happen to amplify SSTA amplitude. Besides, the solution may also show certain propagation features if initial perturbations are limited in coastal regions and propagate toward a distant coastline so that the blocking effect of the coastline can be ignored. The dispersion relation suggests that the propagating wave of a specified wavenumber is energy dispersive and will decline with a rate that is determined by the net surface heating. The propagation feature may be applied in interpreting observed propagating phenomena.

Previous studies had focused on ENSO STPD (Timmermann et al. 2018; Jin 2022). This new model decomposes the equatorial SSTA into a series of natural spatial modes, each of which has its own natural oscillation. It may also be developed by introducing instability terms, nonlinear terms, stochastic terms, and so on. Therefore, this new model can not only provide an explicit physical paradigm for understanding ENSO but also a useful tool to be developed to address more challenges of ENSO STPD.

Author contributions I am the only author of the manuscript.

Funding This study was jointly funded by the National Natural Science Foundation of China (Grants 42275051) and the Fundamental Research Funds for the Central Universities.

Data availability The SODA version 3.4.2 data used in this study are openly available from the University of Maryland at https://dsrs.atmos.umd.edu/DATA/soda3.4.2/.

Declarations

Competing interests The authors declare no competing interests.

References

An S, Jin F (2011) Linear solutions for the frequency and amplitude modulation of ENSO by the annual cycle. Tellus A 63:238–243

Ashok K, Behera SK, Rao SA, Weng H, Yamagata T (2007) El Niño Modoki and its possible teleconnection. J Geophys Res 112:C11007. https://doi.org/10.1029/2006JC003798
Battisti DS (1988) Dynamics and thermodynamics of a warming event in a coupled tropical atmosphere–ocean model. J Atmos Sci 45:2889–2919
Battisti DS, Hirst AC (1989) Interannual variability in a tropical atmosphere–ocean model: influence of the basic state, ocean geometry and nonlinearity. J Atmos Sci 46:1687–1712
Bejarano L, Jin F (2008) Coexistence of equatorial coupled modes of ENSO. J Clim 21:3051–3067
Boucharel J, Timmermann A, Jin F (2013) Zonal phase propagation of ENSO sea surface temperature anomalies: revisited. Geophys Res Lett 40:4048–4053
Cane MA, Zebiak SE (1985) A theory for El Niño and the Southern Oscillation. Science 228:1085–1087
Cane MA, Zebiak SE, Dolan SC (1986) Experimental forecasts of El Niño. Nature 321:827–832
Capotondi AM, Alexander A, Deser C, McPhaden MJ (2005) Anatomy and decadal evolution of the Pacific subtropical–tropical cells (STCs). J Clim 18:3739–3758
Capotondi A, Wittenberg AT, Kug J, Takahashi K et al (2020) ENSO diversity. In: McPhaden MJ, Santoso A, Cai W (ed) El Niño Southern Oscillation in a changing climate, pp 65–86
Carton JA, Chepurin GA, Chen L (2018) SODA3: a new ocean climate reanalysis. J Clim 31:6967–6983
Chen N, Fang X (2023) A simple multiscale intermediate coupled stochastic model for El Niño diversity and complexity. J Adv Model Earth Syst 15:e2022MS003469
Chen H, Jin F (2020) Fundamental behavior of ENSO phase locking. J Clim 33:1953–1968
Chen N, Fang X, Yu J (2022) A multiscale model for El Niño complexity. Npj Clim Atmos Sci 5:16
Deser C, Alexander MA, Xie S, Phillips AS (2010) Sea surface temperature variability: patterns and mechanisms. Annu Rev Mar Sci 2:115–143
Fang X, Chen N (2023) Quantifying the predictability of ENSO complexity using a statistically accurate multiscale stochastic model and information theory. J Clim 36:2681–2702
Fang X, Mu M (2018) A three-region conceptual model for central pacific El Niño including zonal advective feedback. J Clim 31:4965–4979
Geng L, Jin F (2023a) Insights into ENSO diversity from an intermediate coupled model. Part I: uniqueness and sensitivity of the ENSO mode. J Clim 36:7509–7525
Geng L, Jin F (2023b) Insights into ENSO diversity from an intermediate coupled model. Part II: role of nonlinear dynamics and stochastic forcing. J Climate 36:7527–7547
Geng T, Cai W, Wu L (2020) Two types of ENSO varying in tandem facilitated by nonlinear atmospheric convection. Geophys Res Lett 47:e2020GL088784
Gill AE (1980) Some simple solutions for heat-induced tropical circulation. Q J Roy Meteor Soc 106:447–462
Hirst AC (1986) Unstable and damped equatorial modes in simple coupled ocean-atmosphere models. J Atmos Sci 43:606–632
Hirst AC (1988) Slow instabilities in tropical ocean basin–global atmosphere models. J Atmos Sci 45:830–852
Horel JD (1982) On the annual cycle of the tropical pacific atmosphere and ocean. Mon Weather Rev 110:1863–1878
Jin F (1996) Tropical ocean-atmosphere interaction, the Pacific cold tongue, and the El Niño-southern oscillation. Science 274:76–78
Jin F (1997) An equatorial ocean recharge paradigm for ENSO. Part I: conceptual model. J Atmos Sci 54:811–829
Jin F (1998) A simple model for the pacific cold tongue and ENSO. J Atmos Sci 55:2458–2469
Jin F (2022) Toward understanding El Niño Southern-Oscillation's spatiotemporal pattern diversity. Front Earth Sci-Switz 10:899139. https://doi.org/10.3389/feart.2022.899139
Jin F, Neelin JD (1993) Modes of interannual tropical ocean–atmosphere interaction—a unified view. Part I: numerical results. J Atmos Sci 50:3477–3503
Jin F, Lin L, Timmermann A, Zhao J (2007) Ensemble-mean dynamics of the ENSO recharge oscillator under state-dependent stochastic forcing. Geophys Res Lett 34:L03807. https://doi.org/10.1029/2006GL027372
Jin F, Chen H, Zhao S et al (2020) Simple ENSO models, In: McPhaden MJ, Santoso A, Cai W (ed) El Niño Southern Oscillation in a Changing Climate, pp 119–151. https://doi.org/10.1002/9781119548164.ch6
Kang I, An S (1998) Kelvin and Rossby wave contributions to the SST oscillation of ENSO. J Clim 11:2461–2469
Kang I, An S, Jin F (2001) A systematic approximation of the SST anomaly equation for ENSO. J Meteorol Soc Japan Ser II 79:1–10
Kao H, Yu J (2009) Contrasting eastern-Pacific and central-Pacific types of ENSO. J Clim 22:615–632
Keenlyside N, Kleeman R (2002) Annual cycle of equatorial zonal currents in the Pacific. J Geophys Res 107(C8). https://doi.org/10.1029/2000JC000711
Kug J, Jin F, An S (2009) Two types of El Niño events: cold tongue El Niño and warm pool El Niño. J Clim 22:1499–1515
Larkin NK, Harrison DE (2005a) On the definition of El Niño and associated seasonal average U. S. Weather anomalies. Geophys Res Lett 32:L13705. https://doi.org/10.1029/2005GL022738
Larkin NK, Harrison DE (2005b) Global seasonal temperature and precipitation anomalies during El Niño autumn and winter. Geophys Res Lett 32:L16705. https://doi.org/10.1029/2005GL022860
Levine AFZ, Jin F (2010) Noise-induced instability in the ENSO recharge oscillator. J Atmos Sci 67:529–542
Liu C, Zhang W, Jin F, Stuecker MF, Geng L (2022) Equatorial origin of the observed tropical Pacific quasi-decadal variability from ENSO nonlinearity. Geophys Res Lett e2022GL097903. https://doi.org/10.1029/2022GL097903
McCreary JP (1983) A model of tropical ocean-atmosphere interaction. Mon Weather Rev 111:370–387
McPhaden MJ, Zebiak SE, Glantz MH (2006) ENSO as an integrating concept in Earth science. Science 314:1740–1745
McPhaden, MJ, Busalacchi AJ, Anderson DLT (2010) A TOGA retrospective. Oceanography 23(3) 86–103. https://doi.org/10.5670/oceanog.2010.26
Neelin JD (1989) On the intepretation of the Gill model. J Atmos Sci 46:2466–2468
Neelin JD, Jin F (1993) Modes of interannual tropical ocean–atmosphere interaction—a unified view. Part II: analytical results in the weak-coupling limit. J Atmos Sci 50:3504–3522
Newman M, Shin S, Alexander MA (2011) Natural variation in ENSO flavors. Geophys Res Lett 38:L14705. https://doi.org/10.1029/2011GL047658
Picaut JF, Masia F, du Penhoat Y (1997) An advective-reflective conceptual model for the oscillatory nature of the ENSO. Science 277:663–666
Power S, Colman R (2006) Multi-year predictability in a coupled general circulation model. Clim Dynam 26:247–272
Power S, Lengaigne M, Capotondi A et al (2021) Decadal climate variability in the tropical Pacific: characteristics, causes, predictability, and prospects. Science 374:eaay9165. https://doi.org/10.1126/science.aay9165
Ren H, Jin F (2013) Recharge oscillator mechanisms in two types of ENSO. J Clim 26:6506–6523

Ren H, Jin F, Stuecker MF, Xie R (2013) ENSO regime change since the late 1970s as manifested by two types of ENSO. J Meteorol Soc Japan Ser II 91:835–842
Simon Wang SY, Jiang X, Fosu B (2015) Global eastward propagation signals associated with the 4–5-year ENSO cycle. Clim Dynam 44:2825–2837
Stein K, Timmermann A, Schneider N, Jin F, Stuecker MF (2014) ENSO seasonal synchronization theory. J Clim 27:5285–5310
Suarez MJ, Schopf PS (1988) A delayed action oscillator for ENSO. J Atmos Sci 45:3283–3287
Takahashi K, Karamperidou C, Dewitte B (2019) A theoretical model of strong and moderate El Niño regimes. Clim Dynam 52:7477–7493
Takahashi K, Montecinos A, Goubanova K, Dewitte B (2011) ENSO regimes: reinterpreting the canonical and Modoki El Niño. Geophys Res Lett 38 L10704. https://doi.org/10.1029/2011GL047364
Timmermann A, Jin F (2002) A nonlinear mechanism for decadal El Niño amplitude changes. Geophys Res Lett 29:31–34
Timmermann A, Jin F, Abshagen J (2003) A nonlinear theory for El Niño bursting. J Atmos Sci 60:152–165
Timmermann A, An S, Kug J, Jin F et al (2018) El Niño-Southern Oscillation complexity. Nature 559:535–545
Trenberth KE, Stepaniak DP (2001) Indices of El Niño evolution. J Clim 14:1697–1701
Wakata Y, Sarachik ES (1991) Unstable coupled atmosphere–ocean basin modes in the presence of a spatially varying basic state. J Atmos Sci 48:2060–2077
Wang C (2001) A unified oscillator model for the El Niño-Southern Oscillation. J Clim 14:98–115
Wang C (2018) A review of ENSO theories. Natl Sci Rev 5:813–825
Wang C, Picaut J (2004) Understanding ENSO physics—a review. In: Wang C, Xie SP, Carton JA (ed) Earth's Climate, pp 21–48. https://doi.org/10.1029/147GM02
Weisberg RH, Wang C (1997) A western pacific oscillator paradigm for the El Niño-southern oscillation. Geophys Res Lett 24:779–782
Xie R, Jin F (2018) Two leading ENSO modes and El Niño types in the Zebiak-Cane model. J Clim 31:1943–1962
Xie S, Deser C, Vecchi GA et al (2010) Global warming pattern formation: sea surface temperature and rainfall. J Clim 23:966–986
Xie R, Mu M, Fang X (2020) New indices for better understanding ENSO by incorporating convection sensitivity to sea surface temperature. J Clim 33:7045–7061
Zebiak SE, Cane MA (1987) A model El Niño-southern oscillation. Mon Weather Rev 115:2262–2278